[1.]László Péter KISS

FINITE ELEMENT STUDIES ON THE STABILITY OF THREE–PINNED ARCHES

[1.]Institute of Applied Mechanics, University of Miskolc, 3515 Miskolc–Egyetemváros, HUNGARY

Abstract: The in–plane stability of three–pinned circular arches is addressed. The stiffness of the half–arches can be different. The load is a concentrated force and the model accounts for large deformations. The material is linearly elastic and isotropic. The critical loads are assessed together with the displacements, inner forces and moments to compare the effect of several arch angles and stiffness ratios when the span of the arch is given. In this article, the commercial finite element (FE) software Abaqus is used to investigate the nonlinear planar stability and behaviour of three–pinned arches subjected to a concentrated force at the crown point. The stiffness of the half arches can be different. A very flat, a shallow and a deep arch is compared. In Section 2, the properties of the finite element model are detailed. Numerical findings are presented and detailed in Section 3. After that, the Conclusions and References close the article.

Keywords: arch, stability, nonlinear, three–pinned, inner force

1. INTRODUCTION

Arches have long been used as structural stiffeners as these can span huge distances with favourable mechanical behaviour. Some relevant results about the investigation into the subject are gathered in the likes of [1,2,3].

When it comes to the stability, the number of recent literature sources is vast, see example [4,5,6,7]. Within these articles, the elastic planar stability is addressed. The common thing is that, all these assume nonlinear behaviour but under varying load types (concentrated or distributed force, thermal load, etc.). Linear models happen to be overestimating the buckling loads.

A kind of arches that is much less in the researcher's spotlight is internally hinged ones. Such members have the advantage of not transferring moments between the two contacting sides. An analytical model tackling three–hinged steel arches under mechanical load is presented in [8]. Investigations are extended in [9] with thermal load as well. Another analytical model is given in [10] for shallow arches. Internally pinned concrete filled steel tubular arches are comprehensively analysed in [11].

In this article, the commercial finite element (FE) software Abaqus is used to investigate the nonlinear planar stability and behaviour of three–pinned arches subjected to a concentrated force at the crown point. The stiffness of the half arches can be different. A very flat, a shallow and a deep arch is compared. In Section 2, the properties of the finite element model are detailed. Numerical findings are presented and detailed in Section 3. After that, the Conclusions and References close the article.

2. FE MODEL PROPERTIES

The commercial software Abaqus CAE is used for the parametric studies where the two half–arches can have different stiffness through variation of the cross–sectional geometry and material. The loading is a concentrated vertical force acting at the intermediate pin. The end supports are pins, restraining displacements. Each of the half–arches has constant cross–section and linearly elastic, isotropic material, but these are not necessarily the same on the left and right parts. For this reason, modelling of the whole arch is necessary.

As per Figure 1, the arch has a constant initial radius R. The semi–vertex angle is ϑ. The external load is a concentrated dead load P at the crown, while the arch span is

ISSN 1584 – 2665 (printed version); ISSN 2601 – 2332 (online); ISSN-L 1584 – 2665

$$s = 2R\sin\vartheta \tag{1}$$

and centerline length is

$$L = 2\vartheta R. \tag{2}$$

Properties like cross–sectional area A, moment of inertia I and modulus of elasticity E are constant in segments and are distinguished as A_l, I_l, E_l in $[-\vartheta;0]$ and A_r, I_r, E_r in $[0;\vartheta]$.

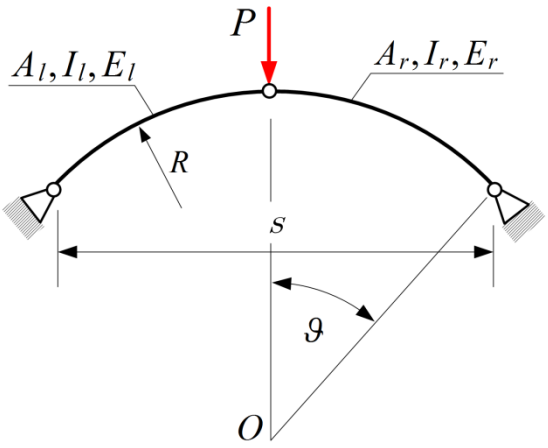

Figure 1. A three–pinned arch

In the Abaqus software, a pin–constraint is applied to model the internal pin between the sides. Arches are mapped with 48 pc. of B21 elements that account for shear deformations. A geometrically nonlinear approach is used with the Static, Riks step to track the nonlinear equilibrium path. The initial external force magnitude is set to 1.

3. FE RESULTS

Numerical studies of this Section include evaluation of the effect of semi–vertex angle and stiffness ratio on the maximum allowable buckling load. At the same time, the displacements, axial force, shear force and bending moments are also assessed. To facilitate the evaluation, let us introduce the radius of gyration on the two sides and their ratio as

$$r_l = \sqrt{\frac{I_l}{A_l}};\ r_r = \sqrt{\frac{I_r}{A_r}};\ \frac{r_r}{r_l} = \hat{r} \tag{3}$$

and the quotient of moment of inertia and modulus of elasticity as follows:

$$\hat{I} = \frac{I_r}{I_l};\quad \hat{E} = \frac{E_r}{E_l}. \tag{4}$$

The cross–section is rectangular. The properties of the left portion are fixed throughout: section width is a=50 mm, height is b=100 mm, modulus of elasticity is 210 GPa. The a dimension is unchanged on the right side, while b is varied. To make comparisons easier, the span is given as 9.735 m. The Poisson ratio is also fixed: 0.3.

As the relative buckling loads are shown in Figure 2, while $\hat{E} = 1$ is kept, this buckling load increases steeply and nonlinearly with $\hat{I}$. Within the plotted range, it can increase by up to almost 30% and decrease by almost 60%. A further important property is that this relationship proves to be independent of the angle in the tested cases: ϑ={0.1;0.4;1.2} [rad].

ISSN 1584 – 2665 (printed version); ISSN 2601 – 2332 (online); ISSN-L 1584 – 2665

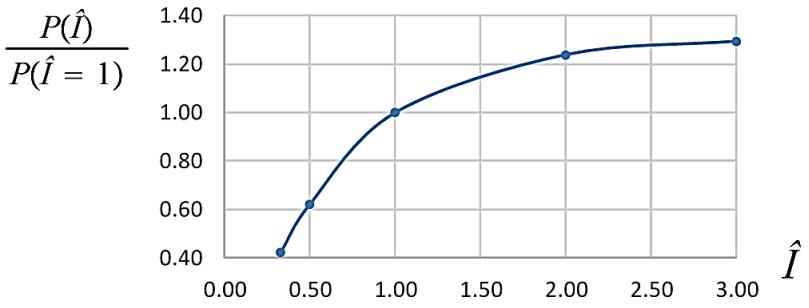

Figure 2. Relative buckling load vs $\hat{I}$

When the elasticity modulus is changed gradually on the right half – $\hat{E}$ =[0.33...1] – it is another nonlinear relationship that is independent of the central angle just like before. The fitting curve for the numerical results is plotted in Figure 3.

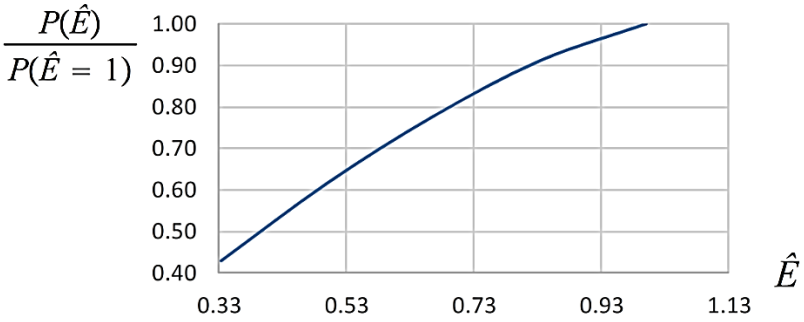

Figure 3. Relative buckling load vs $\hat{E}$

When a very flat (ϑ=0.1) arch bridges the prescribed gap, Figure 4 shows the relative normalized U displacement, N axial force, V shear force and M moment distributions as functions of the φ arc coordinate just before buckling. The plotted values are divided by the maxima when the arrangement is symmetric, i.e., $\hat{I}$=1. As shown, the axial force is almost constant throughout in these selected very flat arches. Although the $\hat{I}$=2 case holds the lowest displacements, it yields the greatest buckling load together with the greatest axial force and moment values. The $\hat{I}$=0.5 case is its direct opposite. The reaction force at the left support is greatest for $\hat{I}$=2, while at the right support is has a peak at $\hat{I}$=1.

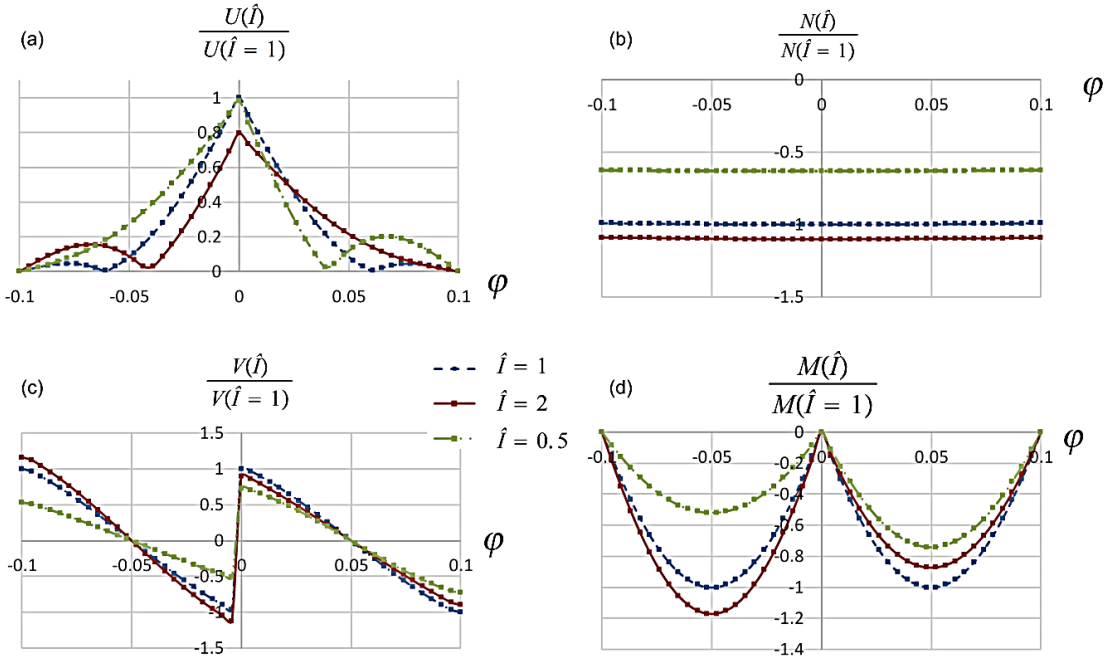

Figure 4. Relative normalized (a) displacement, (b) axial force, (c) shear force, (d) moment for ϑ=0.1

ISSN 1584 – 2665 (printed version); ISSN 2601 – 2332 (online); ISSN-L 1584 – 2665

The exact values for ϑ=0.1 can be read off Figure 5 when the critical (buckling) load is applied and Î=0.33. Figure 5a plots the displacement magnitude in [mm], 5b is the axial force in [N], 5c is the shear force in [N] and 5d reflects the moments in [Nmm]. It can be concluded that maximum displacement occurs at the load application point. Further, the axial force variation is negligible. There is a sudden change in the shear force distribution at the crown point due to the external force. The bending moment is zero at the ends and at the intermediate pin, having a maximum around the middle of the right half arch.

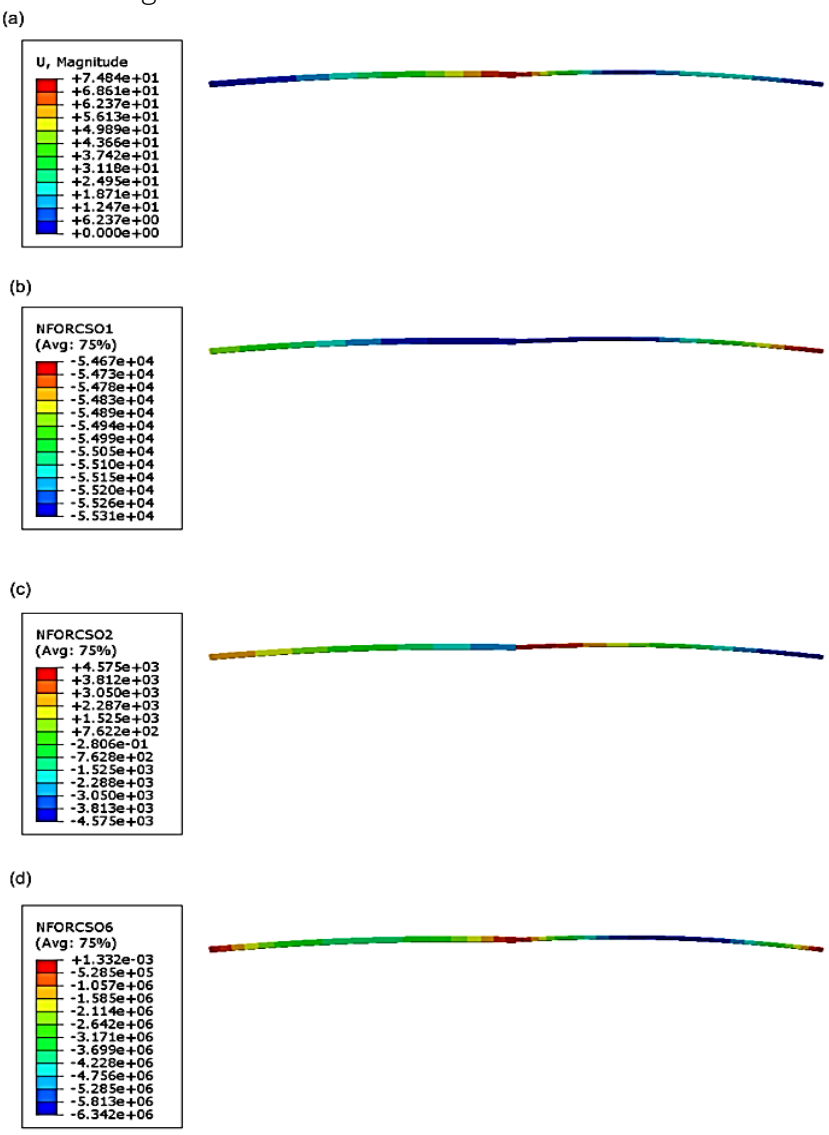

Figure 5. Abaqus (magnified) screenshots just prior to buckling showing (a) displacement, (b) axial force, (c) shear force, (d) moment for ϑ=0.1

Shifting to a shallow arch, namely ϑ=0.4, the same distributions under the same conditions as in Figure 4 are given. Results are graphically shown in Figure 6. This time, the maximum displacement just before buckling for uneven stiffness is lower than in the symmetric case. Moreover, the axial force distribution varies nonlinearly along the angle coordinate. Numerically, the lowest forces and moments appear consistently at Î=0.5, together with the lowest critical load.

Finally, results are shown for a deep arch with ϑ=1.2 in Figure 7. In the maximum displacements, this time, there is no substantial difference. Otherwise, the maximum axial force can change by +29% or the peak moment by +44% compared to the symmetric arch. Around φ=–0.8, the axial force values are almost identical, but the deviation in its vicinity is relatively small. The jump in the shear force reflects the magnitude of the relative buckling load for each case. It can be concluded that the bending moment and shear force distributions are very similar for the three detailed arch angles, while the axial force is clearly the most affected by the arch angle.

ISSN 1584 – 2665 (printed version); ISSN 2601 – 2332 (online); ISSN-L 1584 – 2665

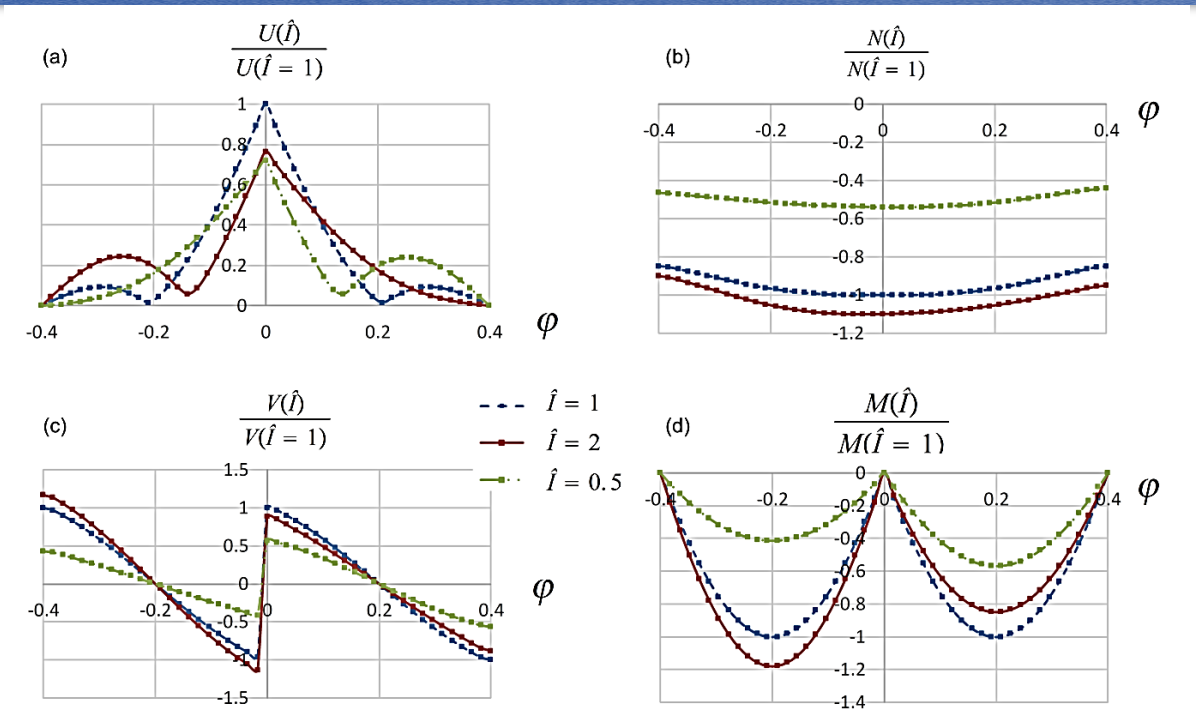

Figure 6. Relative normalized (a) displacement, (b) axial force, (c) shear force, (d) moment for ϑ=0.4

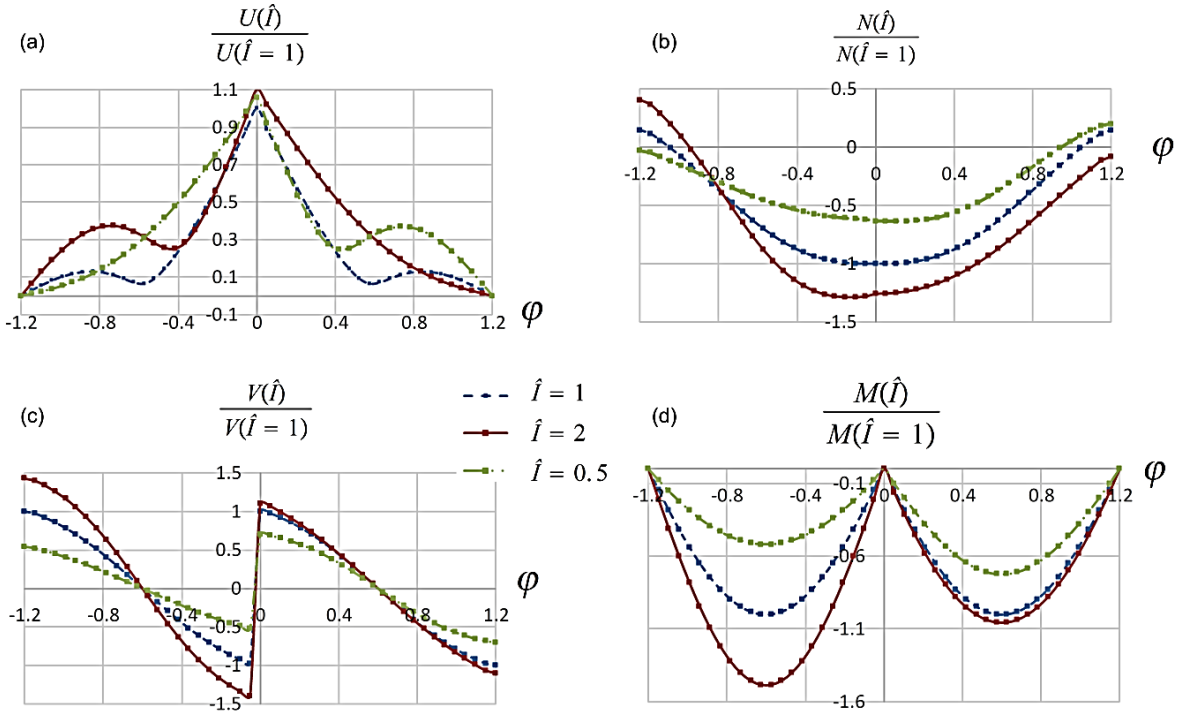

Figure 7. Relative normalized (a) displacement, (b) axial force, (c) shear force, (d) moment for ϑ=1.2

4. CONCLUSIONS

Within this article, the static limit point stability of three–pinned arches was investigated when the stiffness of the half–arches can be different, but constant is each region. A commercial finite element software was used for the computations assuming geometrically nonlinear, physically linear behaviour. The span of the arch was fixed, the angle was varied. It turns out for the selected geometries that the relative buckling load on account of the stiffness change is not affected by the arch angle for rectangular section. Furthermore, stiffer overall geometry possesses greater buckling loads. For three arch angles (referring to very flat, shallow, deep arches) the typical fields were graphically plotted to better understand how these fields change on account of the stiffness and geometry.

ISSN 1584 – 2665 (printed version); ISSN 2601 – 2332 (online); ISSN-L 1584 – 2665

References

[1] Bazant, Z., Cedolin, L.: Stability of Structures. World Scientific, 2010.
[2] Dym, C. L.: Stability Theory and Its Applications to Structural Mechanics. Dover, 2002.
[3] Gönczi, D.: Thermomechanical analysis of functionally graded components using Abaqus. Multidiszciplináris Tudományok: A Miskolci Egyetem Közleménye, 14:4 – 116–124, 2024.
[4] Babaei, H., Kiani, Y., Eslami, M. R.: Thermomechanical nonlinear in–plane analysis of fix–ended FGM shallow arches on nonlinear elastic foundation using two–step perturbation technique. International Journal of Mechanics and Materials in Design, 15:225–244, 2019.
[5] Yan, S.–t., Shen, X., Chen, Z., Jin, Z.: Collapse behavior of non–uniform shallow arches under a concentrated load for fixed and pinned boundary conditions. International Journal of Mechanical Sciences, 137:46 – 67, 2018.
[6] Yan, S.–t., Shen, X., Chen, Z., Jin, Z.: On buckling of non–uniform shallow arch under a central concentrated load. International Journal of Mechanical Sciences, 133:330 – 343, 2017.
[7] Adam, C., Ladurner, D., Furtmüller, T.: In–plane buckling of flexibly bonded three–layer pinned–fixed half–sine shallow arches, International Journal of Non–Linear Mechanics, 151:104369, 2023.
[8] Pi, Y. L. Bradford, M. A.: In–plane analyses of elastic three–pinned steel arches. Journal of Structural Engineering. 141:2 – 06014009, 2014.
[9] Pi, Y. L., Bradford, M. A.: Effects of nonlinearity and temperature field on in–plane behaviour and buckling of crown–pinned steel arches. Engineering Structures. 74:1–12, 2014.
[10] Kiss, L. P.: Stability of arches with internal hinge. Mathematics and Mechanics of Solids. 29:10 – 1947–1957, 2024.
[11] Bradford, M. A., Pi, Y. L.: Geometric nonlinearity and long–term behavior of crown–pinned CFST arches, Journal of Structural Engineering. 141:8 – 04014190, 2015.

ISSN 1584 – 2665 (printed version); ISSN 2601 – 2332 (online); ISSN-L 1584 – 2665